

**Zeeman-limited superconductivity in crystalline Al films**

P. W. Adams

*Department of Physics and Astronomy, Louisiana State University, Baton Rouge, Louisiana 70803, USA*

H. Nam and C. K. Shih

*Department of Physics, The University of Texas at Austin, Austin, Texas 78712, USA*

G. Catelani

*Forschungszentrum Jülich, Peter Grünberg Institut (PGI-2), 52425 Jülich, Germany*

(Received 1 December 2016; revised manuscript received 16 January 2017; published 28 March 2017)

We report the evolution of the Zeeman-mediated superconducting phase diagram (PD) in ultrathin crystalline Al films. Parallel critical field measurements, down to 50 mK, were made across the superconducting tricritical point of films ranging in thickness from 7 to 30 ML. The resulting phase boundaries were compared with the quasiclassical theory of a Zeeman-mediated transition between a homogeneous BCS condensate and a spin-polarized Fermi liquid. Films thicker than  $\sim 20$  ML showed good agreement with theory, but thinner films exhibited an anomalous PD that cannot be reconciled within a homogeneous BCS framework.

DOI: [10.1103/PhysRevB.95.094520](https://doi.org/10.1103/PhysRevB.95.094520)**I. INTRODUCTION**

Tunable spin-imbalance offers a compelling probe of spin correlations, particularly in systems that have a macroscopic ground state that is incompatible with unequal spin populations. This subject has had a long history, but nevertheless, remains at the forefront of condensed matter and atomic physics. In condensed matter one of the most intensely studied examples is that of spin-singlet superconductors subjected to Zeeman and/or exchange fields. In the 1960's, it was proposed that a Zeeman field could induce a spatially modulated order parameter in a spin singlet superconductor, known as the Ferrel-Fulde-Larkin-Ovchinnikov (FFLO) state [1,2]. Over the last decade, substantial thermodynamic evidence for its existence has emerged from studies of ultralow impurity bulk superconductors such as the heavy fermion intermetallic CeCoIn<sub>5</sub> [3,4] and the layered organic superconductors [5–7]. For spintronics applications, the focus is on the interplay between superconductivity and ferromagnetism [8]. For example, spin imbalance can be created in a superconductor by injecting spin-polarized currents from a ferromagnetic metal [9], or a ferromagnetic insulator can induce in the superconductor a large exchange field which can then be modulated by an applied magnetic field [10]. In cold atomic gases, an analog of FFLO has been proposed [11,12] whose behavior is affected by the effective dimensionality of the system. In this paper, we map out, as a function of temperature and film thickness, the Zeeman-limited superconducting phase diagram of crystalline Al films, which are effectively two-dimensional. The phase diagrams of films thinner than 20 monolayers have a structure that markedly differs from that expected for a homogeneous ground state. Our data add further evidence that these otherwise classical BCS superconductors evolve a nontrivial order parameter, that is neither homogeneous nor FFLO, when the Zeeman energy approaches the superconducting gap energy.

The temperature dependence of the parallel (to the film surface) critical magnetic field was measured on epitaxial superconducting Al films, having thicknesses that varied

between 7 ML (17 Å) and 30 ML (72 Å). These thicknesses are much less than superconducting coherence length of the films  $\xi \sim 300$  Å. In this limit, the orbital response to the field is suppressed, and a 1st-order transition to the normal state occurs when the Zeeman splitting is of the order of the superconducting gap  $\Delta_0$  [13]. The conventional picture is that this Zeeman-mediated transition, which is often referred to as the spin-paramagnetic transition, occurs between a homogeneous BCS ground state and a polarized Fermi liquid normal state [14]. The Zeeman critical field is expected to be near the Clogston-Chandrasekhar [15,16] value  $\mu_B H_{cc} = \Delta_0/\sqrt{2}$ , where  $\Delta_0 \approx 1.76k_B T_c$  is the zero temperature gap, and  $\mu_B$  is the Bohr magneton.

**II. SAMPLE PREPARATION**

Epitaxial Al films [18,19] were grown via a two-step method. First, Al was deposited from a Knudsen cell at 0.5 Å/min on a Si(111)-7 × 7 surface which was held below 100 K. After the low-temperature deposition, the films were naturally annealed up to room temperature (RT). Shown in panel (a) of Fig. 1 is an *in situ* STM image of a 10 monolayer (ML) Al film, measured at 77 K, which shows an atomically flat surface interspersed with pits. A profile scan across a pit (see white dash line in Fig. 1) reveals a depth of  $\sim 2.3$  Å, corresponding to a 1-ML depth. Panel (b) of Fig. 1 clearly shows atomic ordering on (111) surface. For the *ex situ* magnetotransport measurements, the epitaxial films were oxidized under an oxygen partial pressure of 1.6  $\mu$ torr for 10 min at RT. This formed a AlO<sub>x</sub> capping layer. Panel (c) of Fig. 1 shows an AFM image that was taken after the surface oxidation of an *in situ* Al film. The silicon step edge and the pit features are clearly resolved, indicating that the capping layer formed without inducing significant damage to the underlying Al film. We believe that the capping layer consumed approximately 3–4 ML of the exposed Al surface [17]. In all of the magnetotransport data presented below, we conservatively estimate the metallic thickness of the films to be 3 ML less than the as-grown thickness. Therefore the quoted

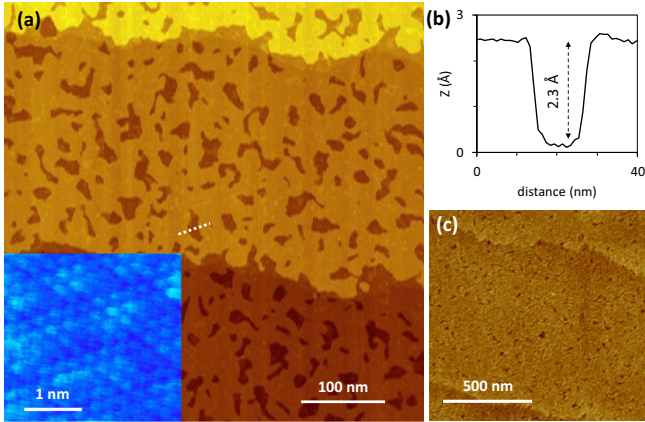


FIG. 1. (a) *In situ* STM image of a 10-ML-thick epitaxial Al film, which shows atomically flat plateaus interspersed with 1 ML-deep pits. (b) Profile trace along the white dash line which crosses over a pit. (c) AFM image of a 10-ML Al film capped by its native oxide.

film thicknesses in the phase diagrams represent an upper bound on the actual metallic thicknesses. Leads were attached to the films by first depositing Cr/Au contact pads via e-beam deposition and then soldering a fine Pt wire to the contact pads with Wood’s metal. The magnetotransport measurements were performed on a dilution refrigerator equipped with a 9-T superconducting solenoid. The films were aligned to parallel orientation with an *in situ* mechanical rotator.

### III. RESULTS AND DISCUSSION

Previous magnetotransport measurements of the parallel critical field behavior of quench-condensed (QC) Al films revealed a hysteretic first-order critical field transition at temperatures below a tricritical point  $T_{\text{tri}} \sim 600$  mK [20,21]. Near the Zeeman critical field, QC films often exhibit nonequilibrium behavior such as stretched-exponential relaxations and avalanches. Recent tunneling density of states measurements have shown that the avalanches represent irreversible collapses of macroscopic regions of superconductivity, and that they are not associated with magnetic flux jumps [22]. In addition to the unusual dynamics,  $T_{\text{tri}}$  of QC Al films is typically a factor of two smaller than predicted by theory. Because quench condensation produces a highly disordered, granular film morphology in Al [23], one cannot easily assess which characteristics of Zeeman-limited superconductivity are attributable to disorder/morphological influences and which are a fundamental property of the condensate. This issue is particularly pertinent to recent reports that disorder can stabilize a patchwork of FFLO-like superconducting puddles [22,25], despite the fact that it is generally agreed that the classic FFLO phase is suppressed in the presence of even modest disorder [3].

In this study, we have made detailed measurements of the Zeeman-limited superconducting phase diagram (PD) in epitaxial (ET) Al films of varying thickness and disorder. As we show below, not only does epitaxial layer-by-layer growth gives one unprecedented control of sample thickness for these types of studies, but for a given thickness, epitaxial films are substantially less disordered than their QC counterparts. This

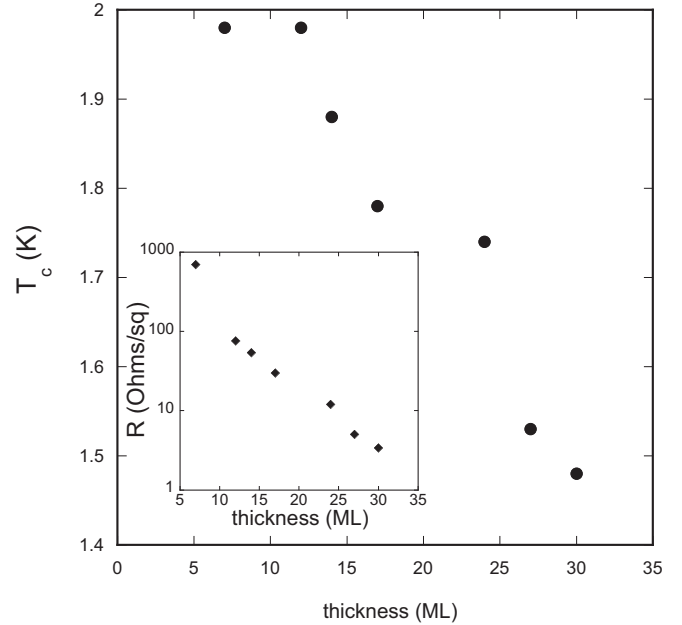


FIG. 2. The transition temperature of the epitaxial Al films used in this study as a function of film thickness and sheet resistance.

offers an unparalleled opportunity to study Zeeman-limited superconductivity in a system whose impurity density is far below what was previously attainable in metal films.

Shown in Fig. 2 are the thickness and resistance dependencies of the transition temperature for a set of films ranging in thickness from 7 to 27 ML. Note that the transition temperature rises rapidly with decreasing film thickness  $t$  until it saturates at  $\sim 2$  K in films with  $t \lesssim 10$  ML. This behavior cannot be attributed to the fact that the sheet resistance itself increases with decreasing  $t$ , see Fig. 2 inset. Generally, amplitude fluctuations of the order parameter in homogeneously disordered superconducting films result in a reduction of  $T_c$  as the films are made thinner and more resistive [24].

The crystallinity of the ET films is reflected in the fact that their sheet resistances are a factor of 2–3 times *lower* than comparably thick QC films. The differing disorder levels between these two types of films is also evident in their respective perpendicular critical field,  $H_{c2}$ , behavior. For comparison, we produced a QC Al film, which had the same as-deposited thickness (48 Å) as the 12-ML ET sample used in this study. We assume that the two samples developed oxide layers of similar thickness and that the mean free path  $l_o$  of each was much less than their respective coherence lengths. In this “dirty limit”,  $H_{c2} = \frac{\Phi_o}{2\pi\xi_o l_o}$ , where  $\Phi_o$  is the flux quantum, and  $\xi_o \sim 1600$  Å is the BCS coherence length of bulk Al [26]. The QC film had a transition temperature  $T_c = 2.4$  K, normal state sheet resistance  $R = 84$  Ω, and  $H_{c2} = 2.0$  T as measured at  $T = 0.5$  K. In contrast, the 12-ML ET film had a  $T_c = 2.0$  K,  $R = 30$  Ω, and  $H_{c2} = 0.28$  T, see inset of Fig. 3. From these data, we can extract the respective ratios of the Pippard coherence length and the mfp for the two types of films:  $\xi^{\text{ET}}/\xi^{\text{QC}} \sim 3$  and  $l_o^{\text{ET}}/l_o^{\text{QC}} \sim 6$ .

Figure 3 shows an example of a typical resistive parallel critical field transition of a 17-ML Al film taken at 90 mK.

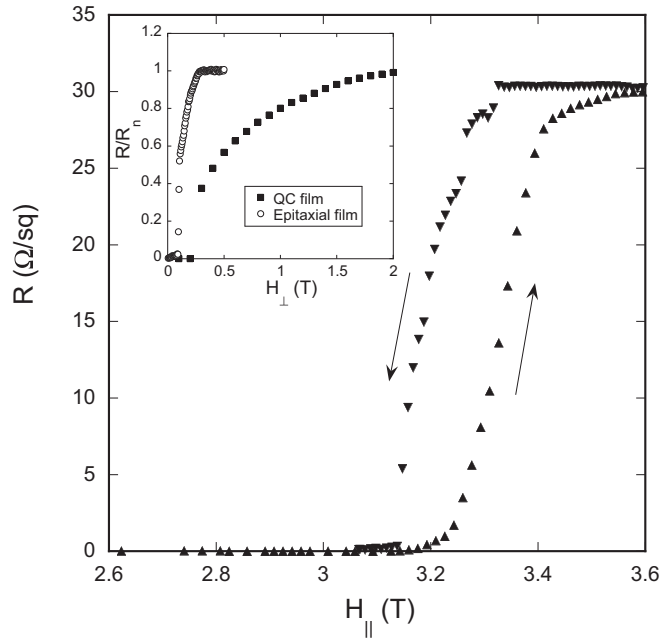


FIG. 3. Hysteretic parallel critical field transition of a 17 ML epitaxial Al film at 90 mK. The arrows depict the magnetic field sweep direction. Inset: Perpendicular critical field transition of a 12-ML epitaxial Al film and a comparably thick quench-condensed Al film.

The hysteresis is indicative of the first-order transition, which was observed in all of the films studied except the 30-ML sample. In contrast to QC films, we found no evidence of avalanches in the critical field traces of any of the samples in this study. By measuring the hysteresis loops as a function of temperature and thickness, one can map out the entire Zeeman-limited PD. We define the critical field at the midpoint of the transition and then plot the temperature dependence of the up-sweep (superheating) and down-sweep (supercooling) critical fields. Although the midpoint criterion is arbitrary, the overall structure of the resulting phase diagrams does not vary significantly when one uses a different criterion for  $H_c$  such as when the resistance reaches 10% of the normal state resistance or when it reaches zero (see Ref. [27] for further discussion). In addition to the finite width of the critical field transitions, the analysis is complicated by the fact that, in the hysteretic region, the films are in a metastable state and therefore exhibit some temporal relaxation. Because of this, the width of the hysteresis loops is a weak function of the magnetic field sweep rate. Slower sweep rates produce slightly narrower hysteresis loops. However, the salient features of the phase diagrams remain unchanged when the sweep rate is varied.

Figure 4 shows the resulting PD of six samples that range in thickness from a few monolayers to 30 monolayers. The abscissa scale of each panel is the same. The triangular symbols are the measured reduced critical fields, which are normalized by the superconducting gap  $\Delta = 1.76k_B T_c$ . The upward triangles (red symbols) represent the superheating phase boundary and the downward triangles (blue) the supercooling boundary. The solid lines are fits to weak-coupling superconductivity theory, which assumes that the transition occurs between

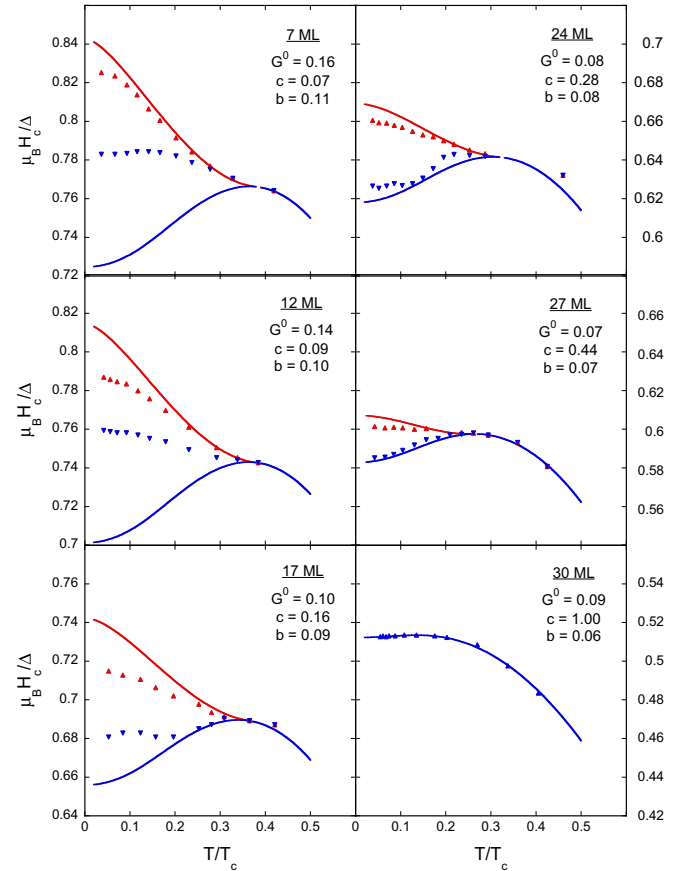


FIG. 4. Zeeman-limited phase diagrams of epitaxial Al films of varying thickness. The symbols represent the superheating (upward triangles) and supercooling (downward triangles) critical fields as a function of reduced temperature. Note that the abscissa field scale is the same for each panel. The superconducting gap was determined from the transition temperature via the BCS relation  $\Delta_0 = 1.74k_B T_c$ . The lines are the theoretic phase boundaries as obtained from QCST by varying  $G^0$ ,  $b$ , and  $c$ . The best fit values of these parameters are listed in the panel legends. The tricritical point is defined by the temperature at which the parallel critical field transition becomes hysteretic.

a homogeneous BCS ground state and a polarized Fermi liquid.

The superconducting properties of thin films in the presence of high Zeeman field are influenced by (1) Fermi-liquid effects which renormalize the spin susceptibility, (2) spin-orbit scattering which inhibits spin polarization, and (3) sample thickness, which determines the relative importance of the orbital response to the magnetic field. The quasiclassical theory of weak coupling superconductivity [28,29] (QCTS), as applied to the Zeeman-limited superconductivity [30–32], captures these effects via the corresponding dimensionless parameters [33]: the antisymmetric Fermi-liquid  $G^0$ , the spin-orbit  $b = \hbar/(3\tau_{so}\Delta_0)$ , where  $\tau_{so}$  is the spin-orbit scattering time, and the orbital pair breaking  $c \propto Dt^2$ , where  $D$  is the electron diffusivity and  $t$  is the film thickness.  $G^0$  is a measure of the renormalization of the spin susceptibility of an interacting Fermi gas. It is related to the ratio of the spin susceptibility density of states  $N_\chi$  to the specific heat density of states [34]  $N_\gamma$  by  $G^0 = N_\chi/N_\gamma - 1$ .

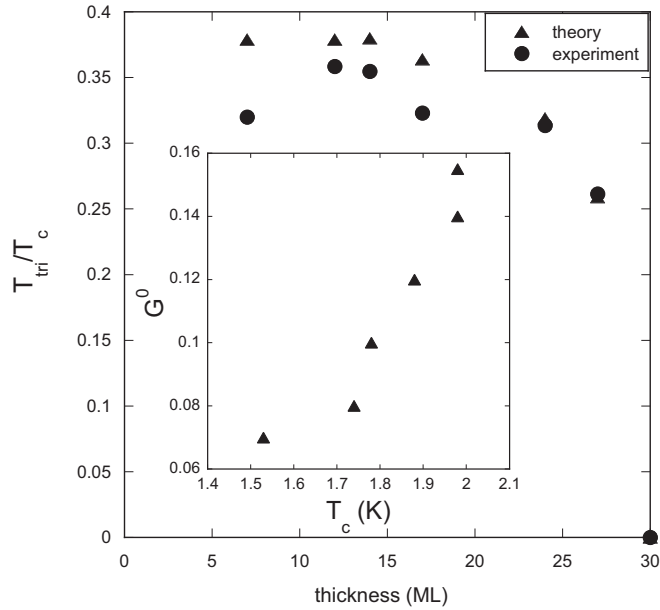


FIG. 5. Reduced tricritical point temperature as a function of film thickness. The triangles were obtained from the QCST fits and the circles from the critical field measurements. (Inset) The antisymmetric Fermi liquid parameter obtained from the QCST fits as a function  $T_c$ .

The QCST traces in Fig. 4 were obtained by varying  $G^0$ ,  $b$ , and  $c$  in order to get the best correspondence to the measured phase diagram. Details of this procedure are provided in Ref. [27]. Following the evolution of the PD's in Fig. 4 from the thickest films to the thinnest, we first note that the critical field transition in the 30-ML sample remains second-order down to the lowest temperatures measured ( $\sim 70$  mK). Also note that there is an excellent agreement between theory and the measured phase boundaries. Furthermore, the extracted values of  $G^0$ ,  $b$ , and  $c$  are consistent with results from studies of relatively thick QC Al films [32]. Interestingly, the spin-orbit parameter  $b$  increases with decreasing thickness, see Ref. [27]. This suggests that a small but measurable spin-orbit scattering rate is associated with the Si-Al interface [35]. Therefore, as the film thickness is lowered, the interface contribution to  $b$  becomes more significant.

The antisymmetric Fermi liquid parameter,  $G^0$ , which accounts for the spin-triplet interaction channel, also increases with decreasing film thickness. The origin of this thickness dependence is unknown, but  $G^0$  does appear to track the thickness dependence of  $T_c$ , see inset of Fig. 5. This implies that the underlying mechanism that gives rise to the enhancement of the spin-singlet interaction channel, which is reflected in  $T_c$  also affects the spin-triplet channel and, consequently, the normal state spin susceptibility.

As can be seen in the 27-ML panel of Fig. 4, decreasing the thickness by only 3 ML reduces the orbital depairing rate enough to open a first-order transition below a tricritical point  $T_{\text{tri}} \sim 380$  mK. Both the tricritical point and the temperature dependence of the hysteresis width  $\Delta H_c(T)$  are well accounted for by the theory. However, as the film thickness is decreased further, the measured PD's begin to deviate more and more

from the theoretical curves. Although QCTS can account for  $T_{\text{tri}}$  across the entire range of thicknesses, see Fig. 5, the measured hysteresis magnitudes are much smaller than expected in the thinner samples. Even more striking, the slopes of the down-sweep branches of the 12-ML and 7-ML PD's are either flat or slightly negative, whereas the slopes of the theory traces are robustly positive. Since the down-sweep critical fields represent the transition from the normal state to the superconducting state, the data in the 12-ML and 17-ML panels indicate that the superconducting phase nucleates well before theory would predict. This behavior is somewhat counterintuitive. It suggests that the nonequilibrium normal state is more fragile than the corresponding superconducting state.

One possibility is that the metastable normal state is simply more susceptible to environmental fluctuations than the superconducting phase which prevents the system from reaching the theoretical supercooling phase boundary. Another possibility is that quantum fluctuations about an intermediate inhomogeneous phase compromise the free energy barrier associated with the first-order transition to the superconducting phase. Indeed, the relative asymmetry of the superheating and supercooling phase boundaries, as compared to the corresponding theory traces, is reminiscent of the asymmetric avalanche behavior observed near the Zeeman critical field of QC Al films [22]. Specifically, highly disordered QC Al films often exhibit avalanchelike jumps in the superheating branch of the hysteresis loop but only very rarely are avalanches observed on the supercooling branch. The absence of supercooling avalanches is consistent with the fact that the supercooling branches of the 7-, 12-, and 17-ML Al films never approach the theoretical limit of metastability.

#### IV. SUMMARY

It is somewhat surprising that the QCST description of the Zeeman-limited PD breaks down in the regime where the orbital pair-breaking contributions are completely negligible. If the films were, in fact, free of disorder, this is precisely the regime where one would expect the FFLO phase to emerge. Interestingly, recent Hubbard model calculations have shown that near the Zeeman critical field a vestige of an FFLO-like phase is stabilized by a finite impurity density [25,36]. This disordered-LO phase is associated with local modulations of the pairing amplitude which, of course, should exhibit some manifestation in the structure of the PD. We speculate that this inhomogeneous phase is preempting the expected supercooling critical field. Extending the present work to include spin-resolved tunneling probes of the Zeeman-limited condensate may help confirm this possibility.

#### ACKNOWLEDGMENTS

The magnetotransport measurements were performed by P.W.A. with the support of the U.S. Department of Energy, Office of Science, Basic Energy Sciences, under Award No. DE-FG02-07ER46420. Film fabrication and characterization was performed by H.N. and C.K.S. with support from grants ONR-N00014-14-1-0330 and NSF-DMR-1506678. The theoretical analysis was carried out by G.C. with partial support by the EU under REA Grant Agreement No. CIG-618258.

- [1] P. Fulde and R. A. Ferrell, *Phys. Rev.* **135**, A550 (1964).
- [2] A. I. Larkin and Y. N. Ovchinnikov, *Zh. Eksp. Teor. Fiz.* **47**, 1136 (1964) [*Sov. Phys. JETP* **20**, 762 (1965)].
- [3] H. A. Radovan, N. A. Fortune, T. P. Murphy, S. T. Hannahs, E. C. Palm, S. W. Tozer, and D. Hall, *Nature (London)* **425**, 51 (2003).
- [4] G. Koutroulakis, M. D. Stewart, Jr., V. F. Mitrovic, M. Horvatic, C. Berthier, G. Lapertot, and J. Flouquet, *Phys. Rev. Lett.* **104**, 087001 (2010).
- [5] R. Beyer and J. Wosnitza, *J. Low Temp. Phys.* **39**, 225 (2013).
- [6] W. A. Coniglio, L. E. Winter, K. Cho, C. C. Agosta, B. Fravel, and L. K. Montgomery, *Phys. Rev. B* **83**, 224507 (2011).
- [7] B. Bergk, A. Demuer, I. Sheikin, Y. Wang, J. Wosnitza, Y. Nakazawa, and R. Lortz, *Phys. Rev. B* **83**, 064506 (2011).
- [8] J. Linder and J. W. A. Robinson, *Nat. Phys.* **11**, 307 (2015).
- [9] C. H. L. Quay, D. Chevalleir, C. Bena, and M. Aprili, *Nat. Phys.* **9**, 84 (2013).
- [10] Y. M. Xiong, S. Stadler, P. W. Adams, and G. Catelani, *Phys. Rev. Lett.* **106**, 247001 (2011).
- [11] L. Radzihovsky and D. E. Sheehy, *Rep. Prog. Phys.* **73**, 076501 (2010).
- [12] Y. Liao, A. S. C. Rittner, T. Paprotta, W. Li, G. B. Partridge, R. G. Hulet, S. K. Baur, and E. J. Mueller, *Nature (London)* **467**, 567 (2010).
- [13] P. Fulde, *Adv. Phys.* **22**, 667 (1973).
- [14] R. Meservey and P. M. Tedrow, *Phys. Rep.* **238**, 173 (1994).
- [15] A. M. Clogston, *Phys. Rev. Lett.* **9**, 266 (1962).
- [16] B. S. Chandrasekhar, *Appl. Phys. Lett.* **1**, 7 (1962).
- [17] N. Cai, G. Zhou, K. Muller, and D. E. Starr, *Phys. Rev. Lett.* **107**, 035502 (2011); *Phys. Rev. B* **84**, 125445 (2011).
- [18] A. R. Smith, K. J. Chao, Q. Niu, and C. K. Shih, *Science* **273**, 226 (1996).
- [19] H. Liu, Y. F. Zhang, D. Y. Wang, M. H. Pan, J. F. Jia, and Q. K. Xue, *Surf. Sci.* **571**, 5 (2004).
- [20] Wenhao Wu and P. W. Adams, *Phys. Rev. Lett.* **73**, 1412 (1994).
- [21] Wenhao Wu and P. W. Adams, *Phys. Rev. Lett.* **74**, 610 (1995).
- [22] J. C. Prestigiacomo, T. J. Liu, and P. W. Adams, *Phys. Rev. B* **90**, 184519 (2014).
- [23] Wenhao Wu, P. W. Adams, R. L. McCarley, and D. J. Dunaway, *Appl. Phys. Lett.* **65**, 1180 (1994).
- [24] J. M. Valles, Jr., R. C. Dynes, and J. P. Garno, *Phys. Rev. Lett.* **69**, 3567 (1992).
- [25] Y. L. Loh, N. Trivedi, Y. M. Xiong, P. W. Adams, and G. Catelani, *Phys. Rev. Lett.* **107**, 067003 (2011).
- [26] M. Tinkham, *Introduction to Superconductivity* (McGraw-Hill, New York, 1996).
- [27] See Supplemental Material at <http://link.aps.org/supplemental/10.1103/PhysRevB.95.094520> for further details of the film characterization and phase diagram analysis.
- [28] G. Eilenberger, *Z. Phys.* **214**, 195 (1968).
- [29] A. I. Larkin and Yu. N. Ovchinnikov, *Zh. Eksp. Teor. Fiz.* **55**, 2262 (1968) [*JETP* **28**, 1200 (1969)].
- [30] J. A. X. Alexander, T. P. Orlando, D. Rainer, and P. M. Tedrow, *Phys. Rev. B* **31**, 5811 (1985).
- [31] T. Suzuki, Y. Seguchi, and T. Tsuboi, *J. Phys. Soc. Jpn.* **69**, 1462 (2000).
- [32] G. Catelani, X. S. Wu, and P. W. Adams, *Phys. Rev. B* **78**, 104515 (2008).
- [33] K. Maki, in *Superconductivity*, edited by R. D. Parks (Dekker, New York, 1969), Chap. 18.
- [34] G. Baym and C. Pethick, *Landau Fermi-Liquid Theory: Concepts and Applications* (Wiley, New York, 1991).
- [35] J. Johansson, S. Saito, T. Meno, H. Nakano, M. Ueda, K. Semba, and H. Takayanagi, *Phys. Rev. Lett.* **96**, 127006 (2006).
- [36] Q. Cui and K. Yang, *Phys. Rev. B* **78**, 054501 (2008).